ACS APPLIED MATERIALS & INTERFACES

Research Article

www.acsami.org

Improvement of the SiO_x Passivation Layer for High-Efficiency Si/PEDOT:PSS Heterojunction Solar Cells

Jiang Sheng,[†] Ke Fan,[‡] Dan Wang,[†] Can Han,[†] Junfeng Fang,[†] Pingqi Gao,*[,†] and Jichun Ye*[,†]

[†]Ningbo Institute of Materials Technology and Engineering, Chinese Academy of Sciences, Ningbo 315201, People's Republic of China

[‡]School of Electronic and Information Engineering, Lanzhou Jiaotong University, Lanzhou 730070, People's Republic of China

Supporting Information

ABSTRACT: Interfacial properties currently hinder the performance of Si/organic heterojunction solar cells for an alternative to high-efficiency and low-cost photovoltaics. Here, we present a simple and repeatable wet oxidation method for developing the surface passivation layer, SiO_x, on the Si surface for the fabrication of high-efficiency Si/poly(3,4-ethylene-dioxythiophene):polystyrenesulfonate (PEDOT:PSS) heterojunction solar cells. The uniform and dense SiO_x thin layer introduced by the oxidizing aqueous solution of H_2O_2 or HNO_3 provided the better surface passivation and stronger wettability of the Si surface, compared to those in the native oxide case. These two types of progress helped create a lower defect density at the Si/PEDOT:PSS interface and thus a high-quality p−n junction with a lower interface recombination velocity. As a result, the HNO_3-oxidized device displayed better performance with a power conversion efficiency (PCE) of 11%, representing a 28.96% enhancement from the PCE of 8.53% in the native oxide case. The effects on the performance of the Si/PEDOT:PSS hybrid solar cells of the wet oxidation treatment procedure, including the differences in surface roughness and wettability of the Si substrate, the quality and thickness of the SiO_x, etc., were explored extensively. Such a simple and controllable oxidizing treatment could be an effective way to promote the interfacial properties that are an important cornerstone for more efficient Si/organic hybrid solar cells.

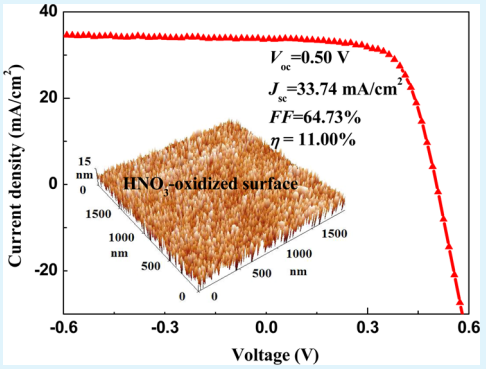

KEYWORDS: *Si/PEDOT:PSS, heterojunction solar cells, wet oxidation, SiO_x passivation, interface modification*

1. INTRODUCTION

Si/organic hybrid solar cells may inherit the advantages of both organic and Si, allowing remarkable potential for low-cost, green, and efficient photovoltaics, because of the adoption of the low-temperature and soluble process. Until now, an encouraging power conversion efficiency (PCE) of above 13% has been reported from Si/poly(3,4-ethylene-dioxythiophene):polystyrenesulfonate (PEDOT:PSS) hybrid solar cells.[1−3] Because the device structure of the Si/PEDOT:PSS hybrid solar cell is rather straightforward, normally composed of front-electrode/p-type PEDOT:PSS/n-type crystalline Si (c-Si)/rear electrode, the PCE is basically determined by the wettability and conductivity of PEDOT:PSS, the absorption of light in the c-Si absorber, the charge transport associated with the interface passivation and morphology, band edge alignment, contact properties, etc. The nonionic surfactant[4] or fluoro-surfactant[5] is used to improve the wettability of the PEDOT:PSS solution. Cosolvents, such as ethylene glycol (EG),[6] dimethyl sulfoxide (DMSO),[7] and methanol,[8] have been reported to be efficient additive agents for improving the conductivity of the coated PEDOT:PSS thin films. Additionally, surface textures (nanowires,[9,10] random pyramids,[11] and hierarchical structure[12]) on the crystalline Si (c-Si) wafer surface are always utilized to suppress light reflection, resulting in improved light harvesting and, thus, the increased photocurrent density (J_{sc}). In the case of band edge modifications, buffer layers with a large band gap, such as Al_2O_3[13] or 1,1-bis[(di-4-tolylamino)phenyl]cyclohexane,[1] are inserted into the interface, to achieve a larger open circuit voltage (V_{oc}) through built-in barrier enhancement. Apart from the PEDOT:PSS and c-Si themselves, the improvements in interfacial properties currently play a crucial role in the PCE.

The inset of a thin dielectric layer, like SiO_x, between the PEDOT:PSS and c-Si will provide the crucial intermediate "i" region for the p−i−n device, which can help to suppress the charge recombination by passivating the Si surface and to promote the collection of electrons by enhancing the internal electrical field.[14] Typically, there are numerous microvoids at the Si/PEDOT:PSS interface, because of the insufficient wettability that leads to a bad surface coverage and severe recombination.[2] The hydrophilic nature of the oxide layer can improve the wettability of the Si surface, which is helpful in the formation of ideal interface contacts between the PEDOT:PSS film and Si substrate, and thus a more ideal p−n junction,

Received: June 19, 2014
Accepted: August 26, 2014
Published: August 26, 2014

 © 2014 American Chemical Society

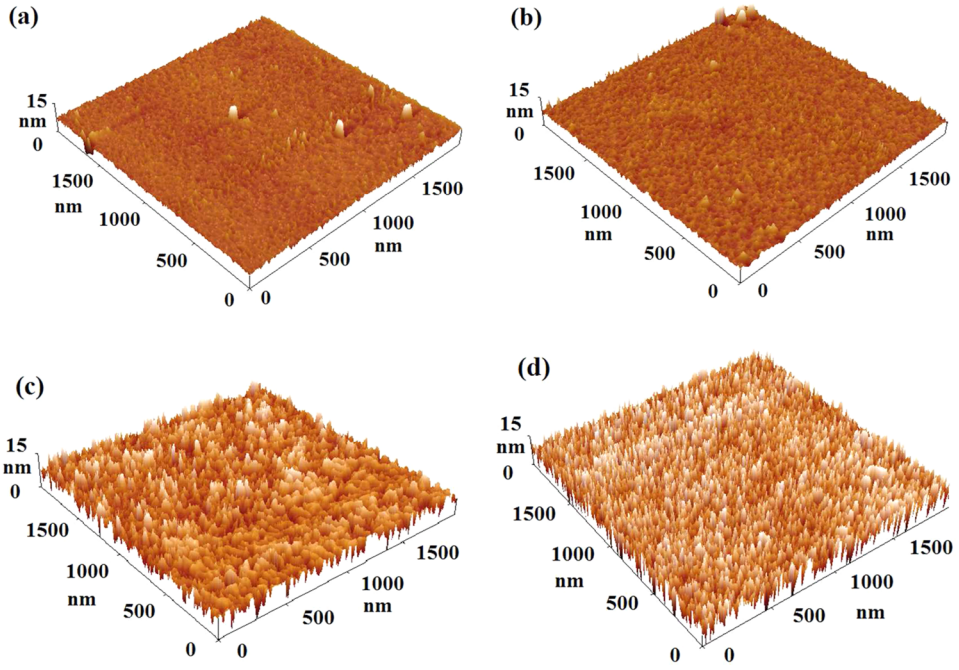

Figure 1. AFM images of silicon surfaces collected from the substrates after the different oxidizing treatments: (a) H−Si surface, (b) HF-etched substrate exposed to the ambient atmosphere for 1 h, and (c and d) HF-etched substrate immersed in the H_2O_2 and HNO_3 solutions for 3 s, respectively.

resulting in less charge recombination and larger photocurrent density.[15,16] For this purpose, the thickness of the oxide layer is a critical parameter. It is insufficient to provide good surface wettability when the SiO_x layer is too thin, whereas the photogenerated carriers have difficulty when they tunnel through the insulating layer once the SiO_x layer is too thick.[17,18] A native oxide layer formed immediately by the exposure of the H-terminated Si substrate to the ambient atmosphere[14,19] is always used to improve the quality of the interface between PEDOT:PSS and Si in the hybrid cell, which results in a photovoltaic performance enhanced compared to that with a bare H−Si surface.[18,19] However, the quality of the native oxide layer is very sensitive to the environmental conditions, including temperature, humidity, oxygen, etc., leading to the variations in surface defect density, hydrophilicity, surface topography, and oxide thicknesses and, thus, the discrepancies in the PCE values of the solar cells. Consequently, it is necessary to develop a controllable method for forming a high-quality SiO_x layer with good uniformity and repeatable thicknesses for application in high-performance Si/PEDOT:PSS heterojunction solar cells.

In this paper, aqueous H_2O_2 and HNO_3 solutions were adopted as the oxidation agents to form appropriate SiO_x layers on the n-type Si surface that were further integrated into the Si/PEDOT:PSS heterojunction solar cells. The characteristics of the SiO_x layers were investigated extensively, including the roughness, hydrophilicity, thickness, and surface topography. The H_2O_2 (HNO_3)-oxidized SiO_x layers were denser and more hydrophilic with a larger surface coverage on the silicon surface, compared to that of the native oxide layer. Meanwhile, the p−n junctions with H_2O_2 (HNO_3)-oxidized surfaces had a good interface connection between Si and the PEDOT:PSS thin film, providing a good junction interface for suppressing the carrier recombination significantly. As a result, the Si/PEDOT:PSS heterojunction solar cells with the H_2O_2 (HNO_3) treatments demonstrated more excellent photovoltaic performance, embodied by a high average PCE of 10.48% for the HNO_3-oxidized device under the simulated solar illumination (AM 1.5, 100 mW/cm^2).

2. EXPERIMENTAL SECTION

The n-type (100) single-side polished, float zone (FZ) Si wafers (resistivity, 3−5 Ω cm) with a thickness of 300 ± 15 μm were cut into 20 mm × 20 mm squares as the substrates. The Si substrates were first cleaned by being rinsed sequentially in acetone, ethanol, and deionized water. Then they were immersed in a solution composed of H_2SO_4 (98%) and H_2O_2 (30%) in a volume ratio of 1:3 at 100 °C for 15 min to remove any possible organic residues. Again, they were placed in a solution that consisted of HCl (37%), H_2O_2 (30%), and deionized water in a volume ratio of 1:1:8 at 80 °C for 15 min to remove metallic residues. Finally, the wafers were immersed in a dilute HF (5%) solution for 3 min to remove the native oxide, receiving H−Si surfaces. The cleaned Si substrates were immediately transferred into the H_2O_2 (10%) or HNO_3 (10%) solution to form the SiO_x thin film.[20,21] The study of the immersion time was conducted for the optimal thickness of the SiO_x layer to obtain the highest-efficiency solar cells (see Figures S3 and S4 of the Supporting Information). It was noted that the devices with a 3 s HNO_3 treatment showed the best photovoltaic performance. A HF-etched sample was exposed to the ambient atmosphere for 60 min to form a thin native SiO_x layer as a reference. A highly conductive PEDOT:PSS (Clevios PH1000) solution mixed with the dimethyl sulfoxide (DMSO, 5%) and Zonyl fluorosurfactant (0.1%) was then spin coated on the SiO_x-terminated Si substrate at a spin speed of 1000 rpm for 60 s. The samples were annealed on a hot plate at 140 °C for 10 min to remove the solvents to form the highly conductive p-type organic thin film. A 150 nm thick Ag film was thermally evaporated to form a grid configuration as the front contact, as seen in Figure S1 of the Supporting Information. Finally, the Ti/Ag layer with a 200 nm thickness was deposited by magnetron sputtering to fully cover the rear side of the Si substrate to form an ohmic contact.

The surface topography and roughness of the silicon wafers were observed by atomic force microscopy (AFM) in a Digital Instruments Dimension 3100 Nanoscope IV. Reflectivity measurements were taken with a spectrophotometer (Helios LAB-rc, with an integrating sphere)

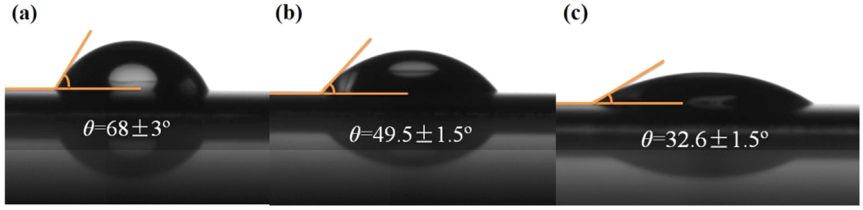

Figure 2. Photographs of water drops on the silicon surfaces after the different oxidation treatment: (a) native oxide surface, (b) H_2O_2-oxidized surface, and (c) HNO_3-oxidized surface.

over a wavelength range of 400−1100 nm. The chemical characteristics of silicon surfaces were measured by attenuated total reflectance Fourier transform infrared spectroscopy (ATR-FTIR, Harrick) and X-ray photoelectron spectroscopy (XPS, AXIS Ultra DLD). Using spectroscopic ellipsometry (Uvisel, Horiba), the thickness of the SiO_x layer was measured. The contact angles were measured by fitting a mathematical expression to the shape of the drop and then calculating the slope of the tangent to the drop at the liquid−solid−vapor (LSV) interface line (Drop Shape Analyzer, DSA100, Kruss). The minority carrier lifetimes of wafers were characterized by a microwave photoconductance decay (μ-PCD) technique (WT2000PVN, Semilab). The current density−voltage (J−V) characteristics of the solar cells were recorded with a Keithley 2400 digital source meter (Keithley) under simulated sunlight (100 mW/cm^2) illumination provided by a xenon lamp (Oriel) with an AM 1.5 filter. The irradiation intensity was calibrated by a standard silicon photovoltaic device (Oriel, model 91150V). The cells were shielded by the opaque mask with an open area of 0.6 cm × 0.6 cm, while the active area of the device was 0.25 cm^2, subtracted the shading area of Ag grids (0.11 cm^2). The temperature was actively controlled at 25 ± 0.5 °C during the measurements. The external quantum efficiency (EQE) system used a 300 W xenon light source with a spot size of 1 mm × 3 mm that was calibrated with a silicon photodetector also from Newport.

3. RESULTS AND DISCUSSION

3.1. Silicon Surface Topography. After the native oxidation layer had been removed via HF etching, the AFM study was conducted, and a typical image of the H-terminated surface is shown in Figure 1a. The surface was quite smooth with a small roughness of 0.554 nm. The AFM images of the SiO_x layers obtained from the different oxidation processes are shown in Figure 1b−d. Exposed to an ambient atmosphere for 1 h after being HF-etched, the nano dimples appeared to be formed on the native oxide surface of the reference sample, as illustrated in Figure1b. The roughness of the native oxide layer was 0.587 nm, slightly larger than that of the H−Si surface, and its surface area ratio (S_{dr}) was 1.22. Panels c and d of Figure 1 show the surface structures of H-terminated Si substrates after immersion in the aqueous H_2O_2 and HNO_3 solutions for 3 s, respectively. There were a large number of peaks in Figure 1c, with a density of summits of 394 cm^{-2}. The roughness and S_{dr} of the H_2O_2-treated surface were 0.912 nm and 3.56, respectively, larger than those of the native oxide surface. For the HNO_3 treatment sample, the surface became much rougher, with a large density of summits of 508 cm^{-2}, a roughness of 1.210 nm, and an S_{dr} of 8.62, 7 times the value for the native oxide surface. The rougher surface would deliver a larger contact area between the substrate and organic film to improve the efficiency of photogenerated carrier separation, if the surface could be well wetted. The wettability of the substrate by the PEDOT:PSS was associated with the hydrophilic property of the SiO_x layer, which will be addressed in the next section. However, the rougher surfaces caused by the oxidizing solutions did not induce any noticeable impact on the light absorption of the substrates (Figure S2 of the Supporting Information). Furthermore, the thicknesses of the SiO_x layers obtained by three different treatments were analyzed by spectroscopic ellipsometry with similar values, 1.40 ± 0.05 nm, which were suitable for the charge tunneling through.[18]

3.2. Wettability of the Silicon Surface. To understand the hydrophilicity of substrates, the water contact angles (θ) collected from the three types of substrate surfaces were measured, as shown in Figure 2. The θ values for the native oxide layer, the H_2O_2-oxidized surface, and the HNO_3-oxidized surface were 68 ± 3°, 49.5 ± 1.5°, and 32.6 ± 1.5°, respectively. Although the H-terminated surface modified by the native SiO_x layer could improve the hydrophilicity, the θ value was still high. Compared to the native oxide layer, there were 27.2% and 52.1% reductions in the water contact angles for the H_2O_2-treated surface and the HNO_3-treated surface, respectively. The remarkably increased wettability of the Si surfaces caused by the treatment of the oxidizing solutions would help to promote the easy spreading of the PEDOT:PSS aqueous solution on the substrate and finally to cover it completely. As a result, the number of surface defects of PEDOT:PSS, such as microvoids, which were always formed during the spin-coating process, could be remarkably reduced. As reported elsewhere, the surface topographic features could affect the contact angle to some extent.[22,23] The rougher surface nanotopography introduced by the oxidizing aqueous solution here would also favor the coverage of the PEDOT:PSS film on the silicon surface. Thus, the Si/PEDOT:PSS junction with the HNO_3-treated surface would be expected to have the best interfacial quality among these three types of oxidation processes.

3.3. Chemical Characteristics of the Silicon Surface. To assess the chemical characteristics of the silicon surfaces after the oxidizing treatments, the various oxide layers were effectively characterized by ATR-FTIR, as illustrated in Figure 3. All the ATR-FTIR absorption curves showed a dominant absorption feature around 1100 cm^{-1} that can be ascribed to the asymmetric stretching vibration of Si−O−Si groups.[24] The peak around 610 cm^{-1} was from the Si−O−Si symmetric stretch of SiO_2.[25] A weak peak at 880 cm^{-1} was Si_2O_3 of the SiO_x thin film. The intensities of Si−O−Si vibrational bands in the specimens for the different oxidation processes were identical. Si oxidation occurred preferentially at the surface near Si−Si bonds, while the Si−H bonds remained intact in the 2071−2252 cm^{-1} region because they were kinetically inert.[20] It should be attributed to the polarity of the O_3Si−H band at 2250 cm^{-1} and the Si−H_3 peak at 2135 cm^{-1}. The associated oxygen atoms with Si−O groups made the silicon surface hydrophilic. Additionally, H_2O molecules were also adsorbed onto the oxidized silicon surface via the aqueous solution, which resulted in peaks of free water in the region of 3580−3670 cm^{-1} and around 1650 cm^{-1} peaks of crystal water.[25] The

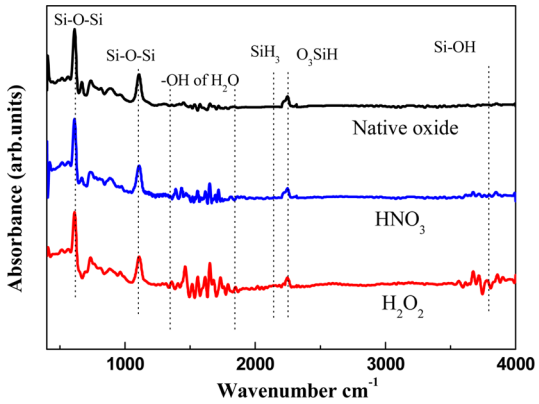

Figure 3. ATR-FTIR absorption spectra of the SiO_x thin films after the different oxidizing treatments.

O−H concentration also increased after the samples had been rinsed with water.[21] The H_2O_2 (HNO_3)-oxidized surfaces presented weak O−H vibrational bands around 3750 cm^{-1}, representing the Si−OH group. Because of a higher intensity for the H_2O_2-treated surface, this oxide layer had more water molecules than that of the HNO_3-oxidized surface. Furthermore, the intensity of O−H groups from the surfaces treated with the aqueous solution was higher than that of the native oxide layer. The presence of O−H groups in the SiO_x layer made the silicon surface more hydrophilic. Thus, after Si−Si back bonds and small amounts of the Si−H surface species had been oxidized, the oxidized silicon surface became more hydrophilic, because of the presence of the oxygen in various bonds, including Si−O and O−H bonds.

The chemical compositions and contents on the silicon surfaces for the different oxidizing samples were also characterized by XPS, as shown in Figure 4. After oxidation, the Si−Si and Si−H bonds were oxidized. The peak of O 1s spectra in Figure 4a was located around 532 eV, which contributed to the components of the O 1s signal from the Si−O group at ~535.50 eV and the Si−OH group at 531.50 eV.[26] The O 1s atomic concentrations for the native oxide layer, H_2O_2-treated surface, and HNO_3-treated surface were estimated to be 9.23%, 12.19%, and 13.84%, respectively. In comparison with the native oxide spectra, the intensity of the O 1s peak from H_2O_2 (HNO_3)-treated surfaces increased remarkably, meaning that there was more SiO_x in the H_2O_2 (HNO_3)-oxidized layers. The Si 2p spectra split into three peaks, the peak from Si−Si of bulk silicon at approximately 99.50 eV, the peak from the SiH_3 group at 99.77 eV, and small amounts of Si(1) (oxidation number of Si given in parentheses, the same below) at 100.31 eV. According to the literature,[20] the signals of oxidized Si between 101.30 and 103.80 eV were attributed to O-containing surface species, in another representation of Si(x). Specific to our case, the peaks of oxidized Si groups located around 102.35 eV were undoubtedly ascribed to Si(3),[20] indicating that the Si(3) species were the main part in the oxide layers. Thus, the composition of the oxide layer was not the SiO_2 crystal, but amorphous SiO_x. The SiO_x content in the different layers followed the same trend as that of the O 1s concentrations in Figure 4b. From the discussion given above, we concluded that the silicon surface had more SiO_x after H_2O_2 (HNO_3) oxidation. Additionally, the SiO_x thin films obtained by the three oxidation processes had the similar thicknesses in comparison, according to the ellipsometry measurement. It meant that the H_2O_2 (HNO_3)-oxidized SiO_x thin films may be denser and their SiO_x coverage on silicon surface may also be greater than that of the native oxide. The strong oxidizing ability of the H_2O_2 (HNO_3) could help the silicon surface to form a high-quality SiO_x passivation layer.

3.4. Photovoltaic Characteristics of Solar Cells. The SiO_x layers from the various oxidation processes exhibited different qualities and properties, which played an important role in the photovoltaic performance of the Si/PEDOT:PSS heterojunction solar cells. The current−voltage characteristics of these heterojunction solar cells with the different SiO_x layers were measured under 100 mW/cm^2 illumination, as shown in Figure 5a. The typical photovoltaic parameters of the three types of hybrid solar cells are summarized in Table 1, including average values and their standard deviation. The H_2O_2-treated solar cell, with a J_{sc} of 33.09 mA/cm^2, a V_{oc} of 0.48 V, and a fill factor (FF) of 60.08%, yielded an average PCE of 9.60%, a 12.54% increase from the value of 8.53% for the native oxide device, while the HNO_3-treated solar cell exhibited the highest average PCE of 10.48%, with a J_{sc} of 33.20 mA/cm^2, a V_{oc} of 0.49 V, and a FF of 64.64%. It was worth noting that the highest PCE of an individual HNO_3-treated device was already beyond 11%. The thickness of the SiO_x layer could be controlled by the chemical treatment time, as shown in Figure S3 of the Supporting Information. For the HNO_3-treated sample, the thickness of the SiO_x layer increased from 1.19 nm for immersion for 1 s to 2.11 nm for immersion for 20 min. A certain thickness of the SiO_x layer was required to have good passivation and good hydrophilicity of the Si surface. However, if the SiO_x layer were too thick, it would impact the

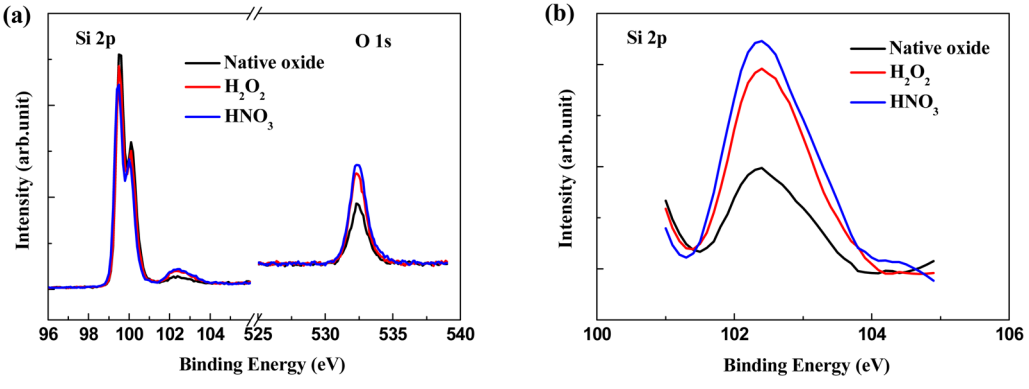

Figure 4. XPS spectra of c-Si (100) surfaces treated by the different oxidizing agents: (a) Si 2p and O 1s region and (b) Si 2p of SiO_x species.

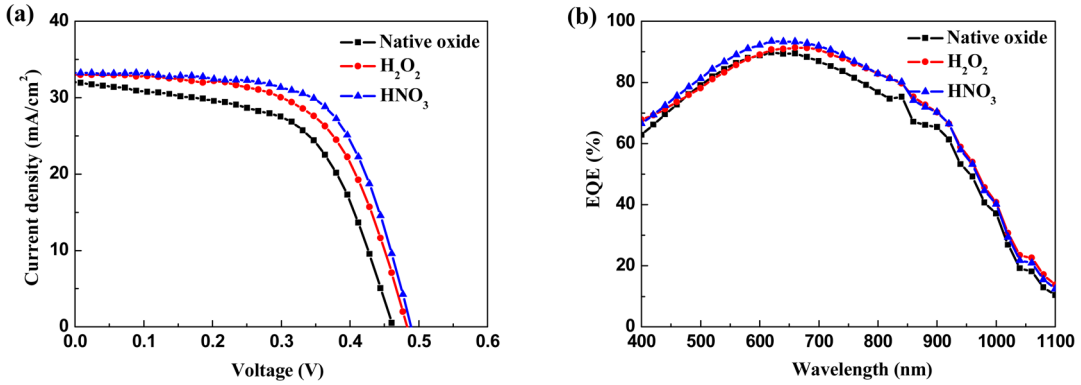

Figure 5. (a) Current density−voltage characteristics of the Si/PEDOT:PSS heterojunction solar cells. (b) External quantum efficiency (EQE) spectra of the fabricated devices based on the different oxidation processes.

Table 1. Photovoltaic Characteristics[a] of Si/PEDOT:PSS Heterojunction Solar Cells with the Different SiO_x Thin Films

	J_{sc} (mA/cm^2)	V_{oc} (V)	FF (%)	η (%)	R_s (Ω cm^2)	R_{sh} (Ω cm^2)
native oxide	32.06 ± 0.50	0.46 ± 0.015	57.56 ± 0.23	8.53 ± 0.40	13.76 ± 0.51	269.89 ± 2.67
H_2O_2	33.09 ± 0.26	0.48 ± 0.011	60.08 ± 0.26	9.60 ± 0.28	12.18 ± 0.45	1257.20 ± 3.74
HNO_3	33.20 ± 0.54	0.49 ± 0.014	64.46 ± 0.27	10.48 ± 0.52	11.00 ± 0.55	2960.64 ± 4.82

[a]Values were obtained by averaging six devices with a calculated confidence interval of 95%.

effectiveness of the carrier tunneling and thus degrade the electrical performance. The duration of the chemical treatment impacted not only the thickness of the SiO_x layer but also the wettability of the surface (surface roughness and hydrophilicity), and other characteristics of the SiO_x layer (such as the film density and content), which would all affect the performance of the device. An optimal thickness of the SiO_x layer could be experimentally determined on the basis of a large amount of experimental data, as shown in Figure S4 and Table S1 of the Supporting Information. The devices with 1.19−1.66 nm SiO_x passivation layers (immersion for 1−10 s) showed superior photovoltaic performance, where the 3 s treatment (corresponding to a 1.4 ± 0.05 nm SiO_x layer) produced the highest efficiency.

Here, the improved photovoltaic performance should be mainly attributed to the thin SiO_x layer oxidized by the aqueous H_2O_2 (HNO_3) solution that enforced the following effects: (1) the improved wettability of the surface of the substrates, which resulted in a better interface contact and thus a higher quality of the p−n junction, and (2) the improved quality, such as the uniformity and density of the SiO_x layers, which promoted the surface passivation to reduce the loss of charge. Specifically, during the HNO_3 oxidation process, the oxide layer might potentially adsorb some cations like NO^+ or NO_2^+, with a large positive surface dipole leading to the improvement in the barrier height of the internal electrical field.[20] This reinforces the fact that the internal electrical field could enhance the driving force for carrier separation, improving the separation efficiency at the interface of the p−n junction and leading to a higher V_{oc}. The obvious evidence was the increase of 30 mV in the V_{oc} of the HNO_3-oxidized device, compared to that of the native oxide device. The increased J_{sc} was mainly caused by the increased Si/PEDOT:PSS interface area, i.e., greater p−n junction area, because of the rougher surface of the H_2O_2 (HNO_3)-treated silicon wafers. The EQE curves of Figure 5b further demonstrate that the H_2O_2 (HNO_3)-treated devices had higher efficiencies on carrier collection. The EQE values of the HNO_3-treated device were slightly larger than that of the H_2O_2-treated device over the full wavelength range, in accordance with the J_{sc} results. Both the J_{sc} and EQE results indicated that the oxide layers formed with the chemical treatment provided better interfacial properties for the Si/PEDOT:PSS heterojunction solar cells. To make the conclusions mentioned above more credible, the surface reflectances of the different samples are shown in Figure S2 of the Supporting Information. Over the broad spectral range of 400−1100 nm, the three samples showed nearly identical reflection properties with an average reflection of 38.7%, indicating that the rougher surfaces from the H_2O_2 (HNO_3) solution did not play a role in light trapping. As shown in Table 1, FF exhibited the largest amplification (the values of the H_2O_2 (HNO_3)-oxidized devices were larger than that of the native oxide device), compared to J_{sc} and V_{oc}. For example, the FF value of the HNO_3-treated device was 12.30% larger than that of the native oxide device. This improvement in FF was revealed by lower series resistances (R_s) and higher shunting resistances (R_{sh}) of devices. The decrease in R_s might be related to the good interface connection, because higher wettability resulted in fewer microvoids at the interface of the PEDOT:PSS film and substrate, allowing a higher efficiency of carrier transport in the lateral direction. The shunt resistance (R_{sh}) was a typical parameter related to defects. The improvement in R_{sh} could be ascribed to the high quality of the SiO_x layer in terms of the uniformity and the density, which would suppress the shunting effectively in the solar cells. In reality, the FF could be also impacted by the diode ideality factor, which will be further discussed in the next paragraph.

To further study the improved performance of cells with the different SiO_x passivation layers, the dark $J-V$ characteristics of solar cells were measured and are plotted in Figure 6. The solar cells fabricated from the Si treated with aqueous H_2O_2 (HNO_3) solutions had dark current densities lower than that of the native oxide cell, while the HNO_3-treated cell carried the lowest value. The dark $J-V$ curves of the Si/PEDOT:PSS heterojunction solar cells exhibited the typical rectifying characteristics, indicating that this heterojunction behaved as well-

dx.doi.org/10.1021/am503949g | ACS Appl. Mater. Interfaces 2014, 6, 16027−16034

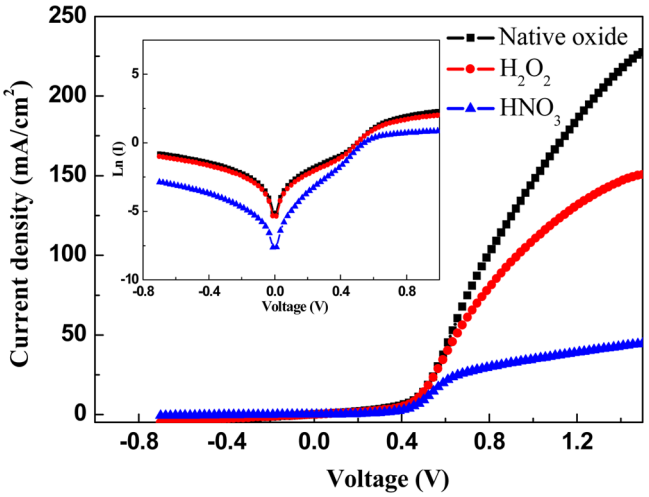

Figure 6. Dark $J-V$ characteristic curves of solar cells based on the different oxidizing devices and ln(J) vs voltage under the dark condition (inset).

defined diodes. The dark $J-V$ curves could be simulated according the diode equations, as follows:

$$J = J_s\left[\exp\left(\frac{eV}{nkT}\right) - 1\right] \quad (1)$$

$$J_s = A^* AT^2 \exp\left(-\frac{\Phi_{bi}}{kT}\right) \quad (2)$$

where A is the contact area, A^* is the effective Richardson constant (~252 A cm^{-2} K^{-2} for n-type silicon), T is the absolute temperature (298 K), κ is the Boltzmann constant, n is the diode ideality factor, J_s is the reverse saturation current density, and Φ_{bi} is the barrier height of Schottky diodes. Equations 1 and 2 were often applied to evaluate the diode ideality factor (n) value of Schottky diodes. From the best fitting of the dark $J-V$ characteristic curves under the forward bias condition (inset of Figure 6), the diode ideality factor, reverse saturation current density, and barrier height of Si/PEDOT:PSS heterojunction solar cells were deduced, as illustrated in Table 2. The n value was a measure of the quality

Table 2. Diode Ideality Factors (n), Reverse Saturation Current Densities (J_s), and Schottky Barrier Heights (Φ_{bi}) of Si/PEDOT:PSS Heterojunction Solar Cells with Different Oxidizing Treatments

surface passivation	n	J_s (μA/cm^2)	Φ_{bi} (eV)
native oxide	2.51	6.56	0.435
H_2O_2	2.24	4.76	0.462
HNO_3	1.68	1.51	0.562

of the p−n junction. The HNO_3-treated solar cell had the smallest n value, which was an indicator of the lowest density of the recombination centers in the space charge region, due to the best passivation quality of the SiO_x layer.[16] Additionally, the J_s values displayed a similar tendency, and the HNO_3-treated device had the smallest value, which was also evidence of weaker carrier recombination with the improved passivation quality of the SiO_x layer. In contrast, the values of Φ_{bi} in the Si/PEDOT:PSS junctions increased with the chemical treatment of the oxidizing aqueous solution, yielding a value of 0.562 eV for the HNO_3-treated solar cell, an increase of 0.127 eV from the value of 0.435 eV of the native oxide solar cell. The increase of Φ_{bi} promoted the J_{sc} and V_{oc} of the Si/PEDOT:PSS heterojunction solar cells, because of the reinforcement of the internal electric field and charge separation force.

3.5. Minority Carrier Lifetimes of Silicon Surfaces. In the previous sections, it had been shown that the SiO_x layer played an important role in the passivation of the Si surface, which could be directly certificated from a spatial mapping of the minority carrier lifetime, as shown in Figure 7. The minority

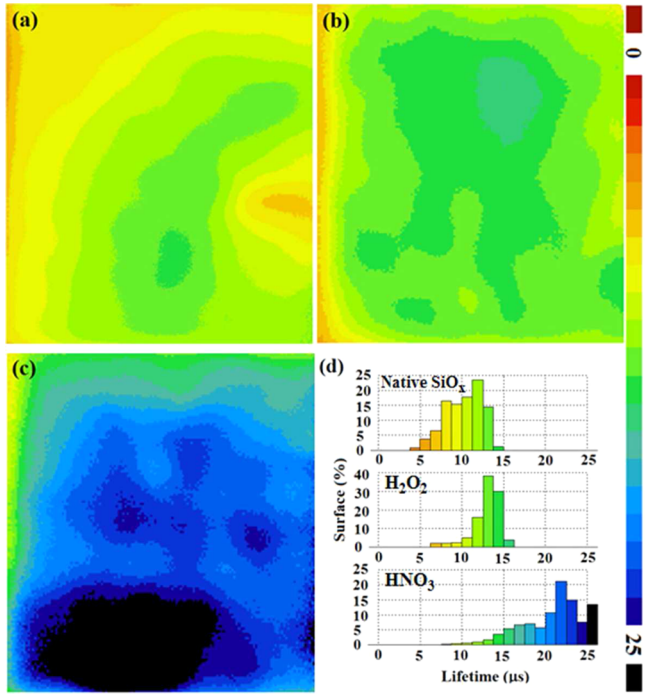

Figure 7. Spatial mapping of the minority carrier lifetimes from the different samples under the various oxidation conditions: (a) native oxide surface, (b) H_2O_2-oxidized silicon surface, and (c) HNO_3-oxidized silicon surface. (d) Histogram of the minority carrier lifetime distribution. The planar silicon wafers were prepared with a 20 mm × 20 mm surface area.

carrier lifetime of a silicon solar cell depends on surface and bulk recombination,[27] which was dominated by the faster process, as expressed in eq 3.

$$\frac{1}{\tau_m} = \frac{1}{\tau_b} + \frac{2S}{d} \quad (3)$$

where τ_m is the measured lifetime, τ_b is the bulk recombination lifetime, S is the surface recombination velocity, and d is the wafer thickness. The native oxide, H_2O_2-treated, and HNO_3-treated substrates had average lifetimes of 10.73, 12.91, and 21.10 μs, respectively. With a 1.43 nm native SiO_x layer, the lifetime distribution of the wafer was broad and the average lifetime was only 10.73 μs, as shown in panels a and d of Figure 7. The passivation quality of the native SiO_x layer was not uniform, due to the thickness and chemical ingredients of the oxide layer. Figure 7b shows the lifetime distribution of the H_2O_2-oxidized surface, with an average lifetime of 12.91 μs, slightly larger than that of the native oxide surface. As seen in panels c and d of Figure 7, the average τ_m value of the HNO_3-oxidized substrate increased to 21.10 μs, and a vast majority of the HNO_3-oxidized surface possesses τ_m values of >20 μs. To

dx.doi.org/10.1021/am503949g | ACS Appl. Mater. Interfaces 2014, 6, 16027−16034

calculate the S values from eq 3, we assumed that all the wafers had a similar d of ~300 μm and a τ_b of 19 ms.[27] The S values were calculated to be 1397, 1161, and 710 cm/s for the native oxide, H_2O_2-treated, and HNO_3-treated surfaces, respectively. Furthermore, these results clearly indicate that the HNO_3-treated surface provides the best passivation properties among the three oxidation methods, which was consistent with the results of XPS analysis (the densest and most uniform SiO_x layer of the HNO_3-treated surface), and also consistent with that of the n, J_s, and V_{oc}, induction of the smallest amount of carrier loss at the interface of Si and PEDOT:PSS.

4. CONCLUSION

In summary, we demonstrated that the H_2O_2 (HNO_3) oxidizing treatment of the Si substrate could improve the surface wettability and passivation property of a high-quality SiO_x layer. This stronger wettability could be ascribed to the greater roughness and hydrophilicity of the SiO_x layer, allowing an effective spread of the PEDOT:PSS coating and thus a good contact between this organic film and the Si substrate. The better interface contact between the rougher Si and the organic film provided a larger p−n junction area. Moreover, the higher SiO_x passivation quality yielded less interface charge recombination. The interfacial improvement by aqueous solution oxidations led to the high-performance Si/PEDOT:PSS heterojunction solar cells, embodied by an excellent PCE of 11% for the HNO_3-treated device. This study not only revealed the roles of the interfacial SiO_x layer in the performance of the Si/organic hybrid devices but also demonstrated the practical importance of such a simple, low-cost, and controllable oxidizing process in the further development of this type of heterojuntion solar cell.

■ ASSOCIATED CONTENT

Supporting Information

Ag grid configuration in the front of the device and reflectance of the fabricated devices based on the different oxidation processes and evidence that the photovoltaic performance of the Si/PEDOT:PSS heterojunction solar cells was dependent on the thickness of the SiO_x layer (the immersion time in the oxidizing solution). This material is available free of charge via the Internet at http://pubs.acs.org.

■ AUTHOR INFORMATION

Corresponding Authors

*E-mail: jichun.ye@nimte.ac.cn. Telephone: 0086-(0)574-87608980.

*E-mail: gaopingqi@nimte.ac.cn. Telephone: 0086-(0)574-86382179.

Notes

The authors declare no competing financial interest.

■ ACKNOWLEDGMENTS

This work was financially supported by the Thousand Talent Program for Young Outstanding Scientists of the People's Republic China, the One Hundred Person Project of the Chinese Academy of Sciences, the Instrument Developing Project of the Chinese Academy of Sciences (Grant yz201328), the National Natural Science Foundation of China (Grant 2140326), the Zhejiang Provincial Natural Science Foundation (Grant LY14F040005), the Natural Science Foundation of Ningbo (Grant 2013A610030 and 2014A610041), and the Zhejiang Province Preferential Postdoctoral Funded Project (BSH1402078).

■ ABBREVIATIONS

PEDOT:PSS, poly(3,4-ethylene-dioxythiophene):polystyrenesulfonate
PCE, power conversion efficiency
J_{sc}, photocurrent density
V_{oc}, open circuit voltage
EG, ethylene glycol
DMSO, dimethyl sulfoxide
AFM, atomic force microscopy
ATR-FTIR, attenuated total reflectance Fourier transform infrared spectroscopy
XPS, X-ray photoelectron spectroscopy

■ REFERENCES

(1) Yu, P.; Tsai, C.-Y.; Chang, J.-K.; Lai, C.-C.; Chen, P.-H.; Lai, Y.-C.; Tsai, P.-T.; Li, M.-C.; Pan, H.-T.; Huang, Y.-Y.; Wu, C.-I.; Chueh, Y.-L.; Chen, S.-W.; Du, C.-H.; Horng, S.-F.; Meng, H.-F. 13% Efficiency Hybrid Organic/Silicon-Nanowire Heterojunction Solar Cell via Interface Engineering. *ACS Nano* **2013**, *7*, 10780−10787.

(2) Thomas, J. P.; Leung, K. T. Defect-Minimized PEDOT:PSS/Planar-Si Solar Cell with Very High Efficiency. *Adv. Funct. Mater.* **2014**, *24*, 4978−4985.

(3) Zhang, Y.; Zu, F.; Lee, S.-T.; Liao, L.; Zhao, N.; Sun, B. Heterojunction with Organic Thin Layers on Silicon for Record Efficiency Hybrid Solar Cells. *Adv. Energy Mater.* **2014**, *4*, 1300923−1300929.

(4) Thomas, J. P.; Zhao, L.; McGillivray, D.; Leung, K. T. High-Efficiency Hybrid Solar Cells by Nanostructural Modification in PEDOT:PSS with Co-solvent Addition. *J. Mater. Chem. A* **2014**, *2*, 2383−2389.

(5) Liu, Q. M.; Ono, M.; Tang, Z. G.; Ishikawa, R.; Ueno, K.; Shirai, H. Highly Efficient Crystalline Silicon/Zonyl Fluorosurfactant-Treated Organic Heterojunction Solar Cells. *Appl. Phys. Lett.* **2012**, *100*, 183901−183905.

(6) Alemu Mengistie, D.; Wang, P.-C.; Chu, C.-W. Effect of Molecular Weight of Additives on the Conductivity of PEDOT:PSS and Efficiency for ITO-free Organic Solar Cells. *J. Mater. Chem. A* **2013**, *1*, 9907−9915.

(7) Liu, Q.; Khatri, I.; Ishikawa, R.; Ueno, K.; Shirai, H. Effects of Molybdenum Oxide Molecular Doping on the Chemical Structure of Poly(3,4-ethylenedioxythiophene):poly(stylenesulfonate) and on Carrier Collection Efficiency of Silicon/Poly(3,4-ethylenedioxythiophene):poly(stylenesulfonate) Heterojunction Solar Cells. *Appl. Phys. Lett.* **2013**, *102*, 183503−183507.

(8) Liu, Q. M.; Imamura, T.; Hiate, T.; Khatri, I.; Tang, Z. G.; Ishikawa, R.; Ueno, K.; Shirai, H. Optical Anisotropy in Solvent-Modified Poly(3,4-ethylenedioxythiophene):poly(styrenesulfonic acid) and its Effect on the Photovoltaic Performance of Crystalline Silicon/Organic Heterojunction Solar Cells. *Appl. Phys. Lett.* **2013**, *102*, 243902−243906.

(9) Sharma, M.; Pudasaini, P. R.; Ruiz-Zepeda, F.; Elam, D.; Ayon, A. A. Ultrathin, Flexible Organic−Inorganic Hybrid Solar Cells Based on Silicon Nanowires and PEDOT:PSS. *ACS Appl. Mater. Interfaces* **2014**, *6*, 4356−4363.

(10) Shen, X.; Sun, B.; Liu, D.; Lee, S.-T. Hybrid Heterojunction Solar Cell Based on Organic−Inorganic Silicon Nanowire Array Architecture. *J. Am. Chem. Soc.* **2011**, *133*, 19408−19415.

(11) Chen, T. G.; Huang, B. Y.; Chen, E. C.; Yu, P. C.; Meng, H. F. Micro-Textured Conductive Polymer/Silicon Heterojunction Photovoltaic Devices with High Efficiency. *Appl. Phys. Lett.* **2012**, *101*, 33301−33306.

(12) Thiyagu, S.; Hsueh, C. C.; Liu, C. T.; Syu, H. J.; Lin, T. C.; Lin, C. F. Hybrid Organic-Inorganic Heterojunction Solar Cells with 12%

Efficiency by Utilizing Flexible Film-Silicon with a Hierarchical Surface. *Nanoscale* **2014**, *6*, 3361−3366.
(13) Pudasaini, P. R.; Ruiz-Zepeda, F.; Sharma, M.; Elam, D.; Ponce, A.; Ayon, A. A. High Efficiency Hybrid Silicon Nanopillar-Polymer Solar Cells. *ACS Appl. Mater. Interfaces* **2013**, *5*, 9620−9627.
(14) Zhang, F.; Sun, B.; Song, T.; Zhu, X.; Lee, S. Air Stable, Efficient Hybrid Photovoltaic Devices Based on Poly(3-hexylthiophene) and Silicon Nanostructures. *Chem. Mater.* **2011**, *23*, 2084−2090.
(15) He, L. N.; Jiang, C. Y.; Wang, H.; Lai, D. N.; Tan, Y. H.; Tan, C. S. Rusli, Effects of Nanowire Texturing on the Performance of Si/Organic Hybrid Solar Cells Fabricated with a 2.2 μm Thin-Film Si Absorber. *Appl. Phys. Lett.* **2012**, *100*, 103104−103108.
(16) Zhang, F. T.; Liu, D.; Zhang, Y. F.; Wei, H. X.; Song, T.; Sun, B. Q. Methyl/Allyl Monolayer on Silicon: Efficient Surface Passivation for Silicon-Conjugated Polymer Hybrid Solar Cell. *ACS Appl. Mater. Interfaces* **2013**, *5*, 4678−4684.
(17) Wei, W. R.; Tsai, M. L.; Ho, S. T.; Tai, S. H.; Ho, C. R.; Tsai, S. H.; Liu, C. W.; Chung, R. J.; He, J. H. Above-11%-Efficiency Organic-Inorganic Hybrid Solar Cells with Omnidirectional Harvesting Characteristics by Employing Hierarchical Photon-Trapping Structures. *Nano Lett.* **2013**, *13*, 3658−3663.
(18) Thomas, J. P.; Zhao, L. Y.; Abd-Ellah, M.; Heinig, N. F.; Leung, K. T. Interfacial Micropore Defect Formation in PEDOT:PSS-Si Hybrid Solar Cells Probed by TOF-SIMS 3D Chemical Imaging. *Anal. Chem.* **2013**, *85*, 6840−6845.
(19) He, L.; Jiang, C.; Wang, H.; Lai, D. Rusli, High Efficiency Planar Si/Organic Heterojunction Hybrid Solar Cells. *Appl. Phys. Lett.* **2012**, *100*, 73503−73507.
(20) Gondek, C.; Lippold, M.; Rover, I.; Bohmhammel, K.; Kroke, E. Etching Silicon with HF-H_2O_2-Based Mixtures: Reactivity Studies and Surface Investigations. *J. Phys. Chem. C* **2014**, *118*, 2044−2051.
(21) Lippold, M.; Bohme, U.; Gondek, C.; Kronstein, M.; Patzig-Klein, S.; Weser, M.; Kroke, E. Etching Silicon with HF-HNO_3-H_2SO_4/H_2O Mixtures: Unprecedented Formation of Trifluorosilane, Hexafluorodisiloxane, and Si-F Surface Groups. *Eur. J. Inorg. Chem.* **2012**, 5714−5721.
(22) Karmouch, R.; Ross, G. G. Experimental Study on the Evolution of Contact Angles with Temperature Near the Freezing Point. *J. Phys. Chem. C* **2010**, *114*, 4063−4066.
(23) Padial-Molina, M.; Galindo-Moreno, P.; Fernández-Barbero, J. E.; O'Valle, F.; Jódar-Reyes, A. B.; Ortega-Vinuesa, J. L.; Ramón-Torregrosa, P. J. Role of Wettability and Nanoroughness on Interactions between Osteoblast and Modified Silicon Surfaces. *Acta Biomater.* **2011**, *7*, 771−778.
(24) Nakajima, A.; Itakura, T.; Watanabe, S.; Nakayama, N. Photoluminescence of Porous Si, Oxidized then Deoxidized Chemically. *Appl. Phys. Lett.* **1992**, *61*, 46−48.
(25) Ay, F.; Aydinli, A. Comparative Investigation of Hydrogen Bonding in Silicon Based PECVD Grown Dielectrics for Optical Waveguides. *Opt. Mater.* **2004**, *26*, 33−46.
(26) Lee, H. J.; Jeon, H.; Lee, W. S. Synergistic Interaction between Substrate and Seed Particles in Ultrathin Ultrananocrystalline Diamond Film Nucleation on SiO_2 with Controlled Surface Termination. *J. Phys. Chem. C* **2012**, *116*, 9180−9188.
(27) Schmidt, J.; Aberle, A. G. Accurate Method for the Determination of Bulk Minority-Carrier Lifetimes of Mono- and Multicrystalline Silicon Wafers. *J. Appl. Phys.* **1997**, *81*, 6186−6199.